ADVANCING EARTH AND SPACE SCIENCE

Geophysical Research Letters

RESEARCH LETTER
10.1029/2020GL088980

**Key Points:**
- We analyze the motion of STEVE and the Picket Fence using the first data obtained from the new Transition Region Explorer True-Color Imager
- The structures within STEVE show a rapid westward motion (~5–10 km/s), compatible with the speed of a fast subauroral ion drift (SAID) channel
- The motion of the Picket Fence is much slower (~400–600 m/s) and can be both westward and eastward, implying a strong flow shear with SAID

**Supporting Information:**
- Movie S1

**Correspondence to:**
J. Liang,
liangj@ucalgary.ca

**Citation:**
Gillies, D. M., Liang, J., Donovan, E., & Spanswick, E. (2020). The apparent motion of STEVE and the Picket Fence phenomena. *Geophysical Research Letters*, *47*, e2020GL088980. https://doi.org/10.1029/2020GL088980

Received 21 MAY 2020
Accepted 3 OCT 2020



# The Apparent Motion of STEVE and the Picket Fence Phenomena

**D. M. Gillies[1], J. Liang[1], E. Donovan[1], and E. Spanswick[1]**

[1]Department of Physics & Astronomy, University of Calgary, Calgary, Alberta, Canada

**Abstract** In this study, we present the first data obtained from the new Transition Region Explorer (TREx) RGB Imager and analyze the apparent motion of STEVE and the Picket Fence structures in an event on 31 August 2019. The structures associated with STEVE are found to feature a fast westward motion (~5–10 km/s). This is consistent with the notions that STEVE is colocated with a fast subauroral ion drift (SAID) channel and that SAIDs play a key role in the production of STEVE. The apparent motion of the Picket Fence structures is much slower (~400–600 m/s) and can be both westward and eastward. This implies that either the Picket Fence is located at different magnetic flux tubes from that of STEVE, with much slower plasma convection speed, or that the motion of the Picket Fence does not follow the plasma convection.

**Plain Language Summary** The recently mounted Transition Region Explorer (TREx) RGB Imager is designed to capture "true color" images of the aurora and airglow with high time resolution and is thus ideal for the identification and tracking of STEVE (pink/mauve) and the Picket Fence (green) phenomena. Using the first data from the new TREx RGB imager at Lucky Lake, Canada, we analyze the apparent motion of STEVE and Picket Fence structures in an event on 31 August 2019. The structures associated with STEVE display a fast westward motion (~5–10 km/s), which is part of the reason for its acronym (*velocity enhancement*). The apparent motions of the Picket Fence structures are much slower (~400–600 m/s) and can be both westward and eastward. The above information on the motion speed of STEVE and the Picket Fence is important to the ongoing exploration of their underlying mechanisms.

## 1. Introduction

A night-sky optical phenomenon named STEVE (*Strong Thermal Emission Velocity Enhancement*) has received much attention in recent years, initially driven by citizen scientists and auroral photography enthusiasts. To date, while its generation mechanism remains more or less subject to speculation, a number of important advancements have been made toward our understanding of STEVE. (1) STEVE is located equatorward of the main aurora zone, and there has been no evidence of appreciable electron/proton precipitation that could be the cause of the luminosity (Gallardo-Lacourt, Liang, et al., 2018; Gallardo-Lacourt, Nishimura, et al., 2018; MacDonald et al., 2018), suggesting that STEVE is not traditional aurora. (2) STEVE was found to be colocated with strong ionospheric electron heating and fast subauroral ion drifts (SAID) (e.g., Spiro et al., 1979) in joint optical and in situ satellite observations (Archer, Gallardo-Lacourt, et al., 2019; Chu et al., 2019; MacDonald et al., 2018; Nishimura et al., 2019). (3) STEVE features distinct color-height distributions. A purple/mauve arc, which often constitutes the visual characteristics of STEVE, is located at a relatively high-altitude range (~210–260 km) (Archer, St.- Maurice, et al., 2019; Liang et al., 2019), while sometimes, a weaker and more whitish STEVE arc may coexist at lower altitudes (~140–180 km) (Archer, St.- Maurice, et al., 2019; Hunnekuhl & MacDonald, 2019; Liang et al., 2019). Another feature, consisting of transient and dominantly green wave-like structures, is the "Picket Fence," often occurs during STEVE intervals but may or may not concurrently coexist with STEVE at a given time. The emission altitude of the Picket Fence is found to be ~110 km, similar to typical auroras (Archer, Gallardo-Lacourt, et al., 2019; Hunnekuhl et al., 2019).

One of the most important breakthrough findings regarding the nature of STEVE was achieved via the recently deployed TREx spectrograph: STEVE is found to contain an overall enhancement of a continuous spectrum spanning between ~400 and 730 nm, that is, an airglow continuum (Gillies et al., 2019; Liang et al., 2019), as its main source of brightness. STEVE may also contain a minor red-line 630 nm emission component, hereby explaining its pink/mauve color, but has small or none out-of-background 557.7 nm green-line emissions. On the other hand, the Picket Fence is dominated by green-line emissions but lack the 427.8 nm blue-line emissions that are usually characteristic of the auroras (Gillies et al., 2019; Mende et al., 2019). So far, based upon available evidence, we (and many research colleagues as per private communications) tend to conceive that neither STEVE nor the Picket Fence is a type of traditional aurora, though their underlying mechanisms remain elusive to date.

The motion velocity of STEVE and Picket Fence structures would undoubtedly offer useful clues to the exploration of their underlying mechanisms. To the authors' knowledge, such a research direction is currently pursued by a few researchers independently, based upon different optical instruments and methodologies. This letter serves two purposes: (1) We shall present the first data obtained from the newly mounted TREx RGB Imager; (2) we shall use the RGB imager data to analyze the motion associated with STEVE and the Picket Fence Phenomena in a case study.

## 2. Instrumentation and Methodology

Images used in this study are from the newly deployed Transition Region Explorer (TREx) True Color Imagers (called "RGB"). TREx is a new multi-instrument observational platform designed to measure multiple optical emissions simultaneously across a swath of geomagnetic latitudes that bracket the foot point of the magnetospheric nightside transition region from dipolar to stretched magnetic topologies. TREx measurements will provide the first ever contiguous picture of the temporal and spatial evolution of auroras and airglows from subauroral to auroral latitudes. The instrument compliment of TREx includes multiwavelength imagers, spectrographs, and RGB imagers. These instruments have the capability to measure or infer the optical spectra of auroras and/or airglows, which is crucial for one to understand the cause and to evaluate the relevant parameters (such as the precipitation energy and fluxes for auroras) of the observed optical phenomena. The direct impact of TREx will be to provide a foundational data set for future satellite missions in relation to magnetospheric remote sensing and magnetosphere-ionosphere-thermosphere (MIT) coupling and provide long-term, spatially resolved information for leading edge models of the MIT. At the time of this writing, TREx is in the deployment stage with some instruments operational and other awaiting installation. First results of the TREx spectrograph were reported in Gillies et al. (2019). In this paper we shall report the first result of the TREx RGB (red green blue) imager. The TREx RGB all-sky imager is a highly sensitive full color imager designed to capture "true color" images of the aurora and airglow. RGB imagers were developed in coordination with Canon Canada Inc. to leverage the Canon ME20F-SH high-sensitivity detector. The ME20 contains a full frame 35 mm CMOS sensor similar to a digital SLR camera but tuned for extreme low light performance. The shutter-less system provides a continuous video feed through an HDMI interface. For TREx RGB, the detector is combined with a fish-eye lens and operated at its slowest frame exposure rate (1/3 s) with a 50 Hz video feed. Custom software systems capture unique frames in the video sequence and provide a software integration of frames to a specified (and dynamically controllable) cadence. In this study, sequences of nine frames are summed to produce 3 s data with an effective 100% duty cycle.

The color response of the system is published (Figure 19) in the Canon White Paper "Advances in CMOS image sensors and associated processing." We note, however, that RGB utilizes the ME20's built-in infrared filter to reduce the long wavelength response of the system. This is done to preserve the color balance and produce images with a similar color response to the human eye. TREx RGB is a network of six cameras installed across central/northern Canada as a compliment to the multispectral imaging framework. The camera utilized in this study is located in Lucky Lake, Saskatchewan (51.15°N, 107.26°W). During this study, the TREx RGB camera was operating at a cadence of 3 s and producing a 558 × 480 pixel true color image. For the purposes of this study, the CCD pixels are then transformed into an Altitude-adjusted Corrected Geomagnetic Coordinate (AACGM) (Baker & Wing, 1989) reference frame for further analysis.

This study uses a data product known as an "ewogram," which is a data product used to analyze zonal motion of auroral and ionospheric forms. Figure 1 provides an example of how we construct an ewogram. A single frame from the RGB camera taken at 06:21:54 UT on 31 August 2019 is mapped in altitude-adjusted corrected geomagnetic coordinates using an assumed emission altitude of 110 km for the Picket Fence Structure. The midlatitude position of the approximate north-south center of the picket fences is manually fitted. As the pickets move equatorward as time progresses, this best fit shifts accordingly. The pixels between −50° and

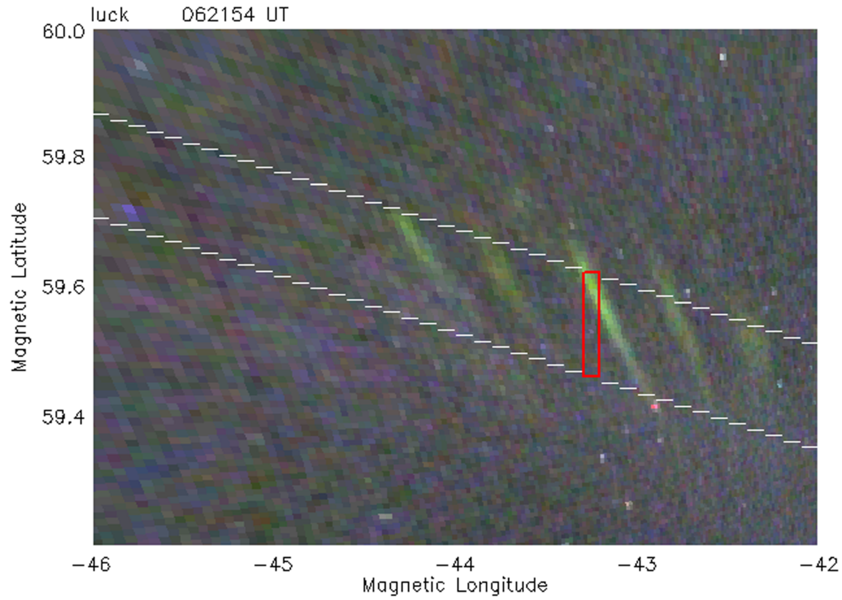


**Figure 1.** Sample image used for the construction of the ewogram figures used in this study. Image captured on 31 August 2019 at 06:21:54 UT in Lucky Lake, SK. Diagonal white lines indicate the upper and lower bounds of the latitude region surrounding the picket fence. The red outline demonstrates the area used to obtain the 97th percentile value of the raw CCD brightness as a function of magnetic longitude.

−30°W magnetic longitude are then divided into 200 longitude bins approximately 0.1° wide and 0.16° in latitude high. Figure 1 demonstrates a sample area of the bin used for each position of AACGM longitude. For each magnetic longitude bin, the 97th percentile value of the raw CCD count is recorded as a function of longitude. The 97th percentile is used instead of the maximum value as an approximate method to filter out particularly bright stars from the dimmer atmospheric structures. This procedure is repeated for each image. Each ewogram slice is rotated to vertical and then stacked in time. The result is visual representation of east-west motion of luminosity as a function time, with magnetic longitude along the vertical axis and time (in UT decimal hours) along the horizontal axis analogous to a traditional keogram.

When an ewogram is constructed, we sample the time-MLON data bins from the ewogram for the slant "trace" of interest according to certain intensity threshold, and the slope (i.e., speed) of the trace is calculated from those data points via a least squares fitting. The error in the speeds estimated from the above ewogram analysis stems from two systematic processes. The first and major source of error arises from uncertainty in the emission heights. The second source of error originates from the inaccuracy in determining the slope of a "trace" of signatures, which consist of a set of scattered pixels in time-MLON bins of the ewogram. For the first error, we assume a height range of ~100–120 km for the Picket Fence according to Archer, Gallardo-Lacourt, et al. (2019) and Hunnekuhl et al. (2019). The altitudes of STEVE are more uncertain since it may consist of two separated layers, each of which may have an ~20–40 km width (Archer, St.- Maurice, et al., 2019; Liang et al., 2019). In the following calculation we assume an altitude range of 190–220 km for STEVE, and the results can be extrapolated to other height ranges. The optical features of interest are mapped to the lower and upper range of the above heights, and the errors are evaluated accordingly. For the second error, the standard deviation of the slope of a set of 2-D data points has a strict mathematical definition (e.g., McCuen, 1985). The error estimates from the above two sources are calculated for all STEVE/Picket Fence structures of interest and listed in Table 1. More details on the technique and error analyses of velocity estimation based upon ewograms, as well as their applications to various optical phenomena, will be the content of a separate paper in the near future.

## 3. A Case Study: 31 August 2019

On the night of 31 August 2019, the RGB imager located in Lucky Lake, SK, observed a STEVE and Picket Fence event. The clearest observation of both features occurred between ~6:10 and 6:40 UT. The

**Table 1**
*Speeds and Associated Error Estimates*

| | | $\sigma_h$ (error from emission altitude) | $\sigma_a$ (error from slope) | $\sigma_{tot}$ (total error) | Speed with error estimate |
|---|---|---|---|---|---|
| Westward Pickets | 1 | 40 m/s | 10 m/s | 41 m/s | 610 ± 41 m/s |
| | 2 | 50 m/s | 23 m/s | 55 m/s | 480 ± 55 m/s |
| | 3 | 60 m/s | 26 m/s | 65 m/s | 460 ± 65 m/s |
| Eastward Pickets | 1 | 80 m/s | 6 m/s | 80 m/s | 380 ± 80 m/s |
| | 2 | 80 m/s | 8 m/s | 80 m/s | 390 ± 80 m/s |
| STEVE | 1 | 0.5 km/s | 0.008 km/s | 0.5 km/s | 6.3 ± 0.5 km/s |
| | 2 | 1.0 km/s | 0.02 km/s | 1.0 km/s | 6.0 ± 1.0 km/s |
| | 3 | 1.1 km/s | 0.02 km/s | 1.1 km/s | 7.0 ± 1.1 km/s |
| | 4 | 0.6 km/s | 0.07 km/s | 0.6 km/s | 5.3 ± 0.6 km/s |
| | 5 | 0.8 km/s | 0.07 km/s | 0.8 km/s | 6.5 ± 0.8 km/s |
| | 6 | 1.1 km/s | 0.05 km/s | 1.1 km/s | 9.6 ± 1.1 km/s |

supporting information shows the time lapse of this event. Figures 2a–2c show sample images used to create the ewograms for analyzing the drift speeds of Picket Fence and STEVE structures (Figures 2d and 2e). An emission altitude of 110 km is assumed for the Picket Fence (Archer, St.- Maurice, et al., 2019; Hunnekuhl & MacDonald, 2019) in Figures 2a and 2b, while an emission altitude of 200 km was assumed for STEVE in Figure 2c based on the results in Archer, St.- Maurice, et al. (2019) and Liang et al. (2019). Note that in Figure 2c the Picket Fence coexists with STEVE but we use the 200 km emission altitude anyway since we only focus on, and sample STEVE, for the ewogram (Figure 2f). As described above, each slice consists of a 0.16° latitudinal width band and a 0.1° longitudinal width bin. Five minutes of data were analyzed for each section, and the results are discussed below. The motion speeds we present below are those mapped to the Earth's surface as implied in AACGM coordinates. Mapping back to the realistic altitudes of phenomena would lead to trivial modification of the speeds that would not affect our overall results.

### 3.1. Apparent Motion of the Picket Fence

The Picket Fence manifests itself as quasiperiodic, and often collimated, columns of optical emissions. With the TREx RGB camera, it is particularly straight forward to identify the Picket Fence. Besides their characteristic morphological features, the Picket Fence exists predominantly in the green channel and shows only a faint imprint (presumably from N2 1PG; see Mende et al., 2019) in the red channel, yet nothing on the blue channel. Due to their primarily green nature, only the green channel of the RGB image was used for the Picket Fence structures. Figure 2d exhibits the apparent westward motion of the Picket Fence structures. The ewogram represents a 5 min time period from ~06:20–06:25 UT. East (west) is toward the top (bottom) of the image, and time is along the horizontal axis. Three Picket Fence structures are sampled, and their drift motion is identified by the black and white dashed arrows. The westward velocities of the picket structures, from left to right, are 610 (±41), 480 (±55), and 460 (±65) m/s.

Later, it was noticed that a portion of the Picket Fence structures began to counterstream in the eastward direction. Again, using just the green channel of the RGB image, a 5 min ewogram from ~06:30–06:35 UT was created and is shown in Figure 2e. Two clear eastward moving green structures were identified, and their drift motion (from left to right) was calculated to be 380 (±80) and 390 (±80) m/s. This motion is slower in magnitude than the westward motion seen earlier. Such slowly eastward moving structures can be discerned in the supporting information during ~06:30–06:40 UT in the western portion of the field of view (FOV).

### 3.2. Apparent Motion of STEVE

Unlike the Picket Fence, STEVE features a broadband optical spectrum that is expected to result in a mixture of red/green/blue channels in RGB images. We chose to focus on the red and blue channels of the camera when building the ewogram for STEVE to reduce the "contamination" from the coexisting Picket Fence. The westward motion of structures along STEVE is shown as bright red in the ewogram beginning at the top of Figure 2f and traveling to the bottom of the figure. Horizontal striations with no apparent change in longitude are stellar bodies. While choosing the 97th percentile value of the raw CCD luminosity we

10.1029/2020GL088980

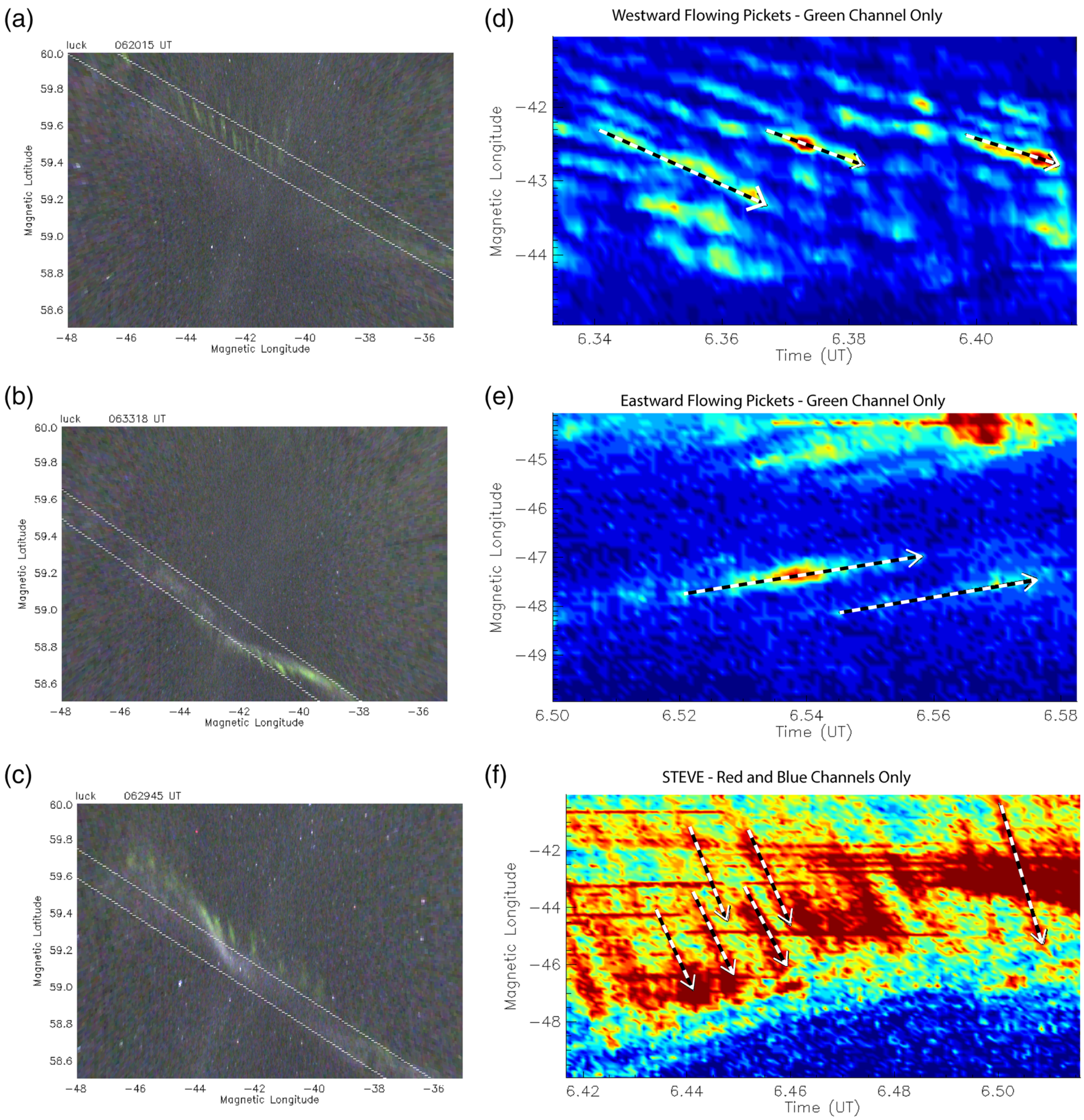


**Figure 2.** Event recorded by the TREx RGB LUCK ASI on 31 August 2019 in Lucky Lake, SK. (a–c) Single frame of images with the latitudinal boundaries used in construction of the ewograms to the right at 06:20:15, 06:33:18, and 06:29:45 UT. (a, b) Pickets mapped to 110 km and converted to a magnetic latitude and longitude coordinates frame. (c) STEVE structure mapped to 200 km and converted to a magnetic longitude and latitude reference frame. Diagonal white lines identify latitudinal spread used in ewogram. Each ewogram was constructed using the luminosity value of the 97th percentile for each magnetic longitude bin. Each bin was 0.16° × 0.1° wide (latitude/longitude). (d–f) Resulting ewogram constructed using 5 min intervals. Magnetic longitude along the vertical axis and time along the horizontal axis. (d) Ewogram depicting zonal (westward) motion of Pickets between 06:20 and 06:25 UT. (e) Ewogram depicting eastward motion of Picket structures between 06:30 and 06:35 UT. (f) Ewogram depicting westward motion of structures within STEVE between 06:25 and 06:30 UT. Individual pickets or STEVE structures identified by dashed black and white arrow.

were able to filter out most stars, it was unable to do a complete removal of the stars from the ewogram. It is straightforward to see that features within STEVE have dominantly westward propagation. Six westward moving structures were sampled, and their respective velocities (from left to right) are estimated to be 6.3 (±0.5), 6.0 (±1.0), 7.2 (±1.1), 5.3 (±0.6), 6.5 (±0.8), and 9.6 (±1.1) km/s. That the STEVE structures move much faster than the coexisting Picket Fence can be readily perceived when one views the supporting information, for example, during ~06:24–06:30 UT.

## 4. Summary and Discussion

We have presented the first data obtained from the new TREx RGB Imager and discussed a case study analyzing the motion associated with STEVE and the Picket Fence. The fine structures on STEVE are found to feature a fast westward motion (~5–10 km/s). This is consistent with the established notion that STEVE is usually colocated with a SAID channel (Archer, Gallardo-Lacourt, et al., 2019; Chu et al., 2019; MacDonald et al., 2018; Nishimura et al., 2019). Though there is no in situ measurement of an SAID in this event, the westward speed of STEVE is compatible in order of magnitude with the reported velocities of an SAID during STEVE intervals. The pending question is how the SAID interacts with the Earth's atmosphere to excite the chemiluminescence airglow continuum that is characteristic of STEVE (Gillies et al., 2019; Liang et al., 2019). Harding et al. (2020) proposed that the nitrogen molecules can be excited to high vibrational levels via the collision with fast-drifting ions in a SAID and may thus overcome the energy barrier in reacting with oxygen atoms to produce NO, which then react with O to generate the $NO_2$ continuum (Sternberg & Ingham, 1972) that accounts for the STEVE airglow continuum. Even though the neutral response and the airglow production may have a finite growth time in response to the SAID ions' passage, assuming the growth time is nearly constant, the successive appearance of STEVE structures at different longitudes would still essentially follow the SAID speed.

The much slower (~400–600 m/s), counterstreaming motion of the Picket Fence is more intriguing. We realize that in another study using citizen scientists' videos, Hunnekuhl et al. (2019) estimated a westward velocity of ~150 m/s for the Picket Fence. The motion speed of the Picket Fence is thus at least an order of magnitude slower than that of STEVE. This result seems not to support the hypothesis that STEVE and the Picket Fence are colocated at *exactly* the same magnetic flux tubes, though they are indeed fairly close to each other. More likely, the Picket Fence is situated adjacent to STEVE flux tubes, and the convection velocity there differs vastly from the SAID. If this is the case, a strong flow shear, which alludes to the presence of a field-aligned current (FAC), must exist in the vicinity of a SAID. It has long been recognized that a SAID is roughly colocated with a local peak of Region 2 downward FAC (e.g., Anderson et al., 2001; Archer, Gallardo-Lacourt, et al., 2019; Figueiredo et al., 2004; He et al., 2014) but the peak FAC density was generally found to be at most ~1 $\mu A/m^2$. While a rigorous triangulation analysis to determine the latitude/height of STEVE and the Picket Fence is not achievable in this study, based upon the so-far recognized emission height range of those structures (Archer, St.- Maurice, et al., 2019; Hunnekuhl et al., 2019; Liang et al., 2019), we estimate that the AACGM latitude difference between STEVE and the Picket Fence is unlikely to be larger than ~0.2°, which is compatible with Archer, Gallardo-Lacourt, et al. (2019) considering the latitudinal resolution of their analysis. When viewing the supporting information, in which we use an emission height of 110 km, one may notice that the Picket Fence initially appears to be at higher latitudes than STEVE, while later when STEVE and the Picket Fence move southward and pass over the station zenith (~59.1° MLAT), the Picket Fence seems to be at lower latitudes than STEVE. This is very likely due to the latitude-altitude aliasing (when a constant emission height is assumed) of a near-vertical distribution viewed from a different perspective. In fact, the observation that STEVE and the Picket Fence appear to largely overlap between ~06:31 and 06:32 UT, implying that they are roughly aligned along the same viewing direction, has helped us derive an estimation of their relative MLAT difference as mentioned above. An ~5 km/s change of convection velocity over 0.2° MLAT with FAC density of ~1 μA/m2 would indicate a height-integrated Pedersen conductance $\Sigma_P$ smaller than 0.1 S. To the authors' knowledge, so far, there is a lack of direct measurements of the ionospheric conductance in the SAID region, and indirect inferences from in situ observations or via models (e.g., Figueiredo et al., 2004; Zheng et al., 2008) often yielded $\Sigma_P$ of order of ~1 s in SAID. To explain the strong flow shear inferred from our observations, either the local FAC intensity is exceedingly high, or $\Sigma_P$ is very low, in the SAID region associated with STEVE. Either of the two conditions is pending for future examinations in realistic observations.

One other possibility lies in that a small-scale yet intense FAC system might be generated purely in the ionosphere, in the presence of a sharp gradient of horizontal electric currents. The possible existence of such a small-scale ionospheric FAC system with intense yet altitudinally confined parallel electric field was first proposed and modeled by St. -Maurice et al. (1996) and later advanced by Noël et al. (2000). Contingent upon the model parameters, the peak FAC intensity may reach hundreds of $\mu A/m^2$ over a narrow width, leading to a strong flow shear of up to a few km/s per km. One other interesting result in their theories is that they predict a parallel electric field on order of a fraction of 1 mV/m, over an altitudinal range of several tens of km between the ionospheric *E* and lower *F* region (see, e.g., Figure 6 in Noël et al., 2000). Assuming an average $E_{//}$of ~0.2 mV/m that spans an altitude range of ~50 km, the resulting electron acceleration would be sufficient to excite the 557.7 nm green line (~4.19 eV) and N2 1PG emissions (~7.35 eV) (Mende et al., 2019), yet not enough to excite the $N_2^+$ 1 N 427.8 nm emission (~18.75 eV). This is consistent with the absence of blue-line 427.8 nm emissions in the Picket Fence spectra (Gillies et al., 2019; Mende et al., 2019). That being said, existing theories and simulations put forth by St. -Maurice et al. (1996) and Noël et al. (2000) are not directly applicable to our research target, since their model condition and assumptions were not designed for the context of SAID and STEVE. It is however noted that a condition of sharp gradients of horizontal currents similar to their models might also exist near the edge of a strong and narrow SAID channel. A revised theoretical model of the generation of small-scale FACs and parallel electric fields in the lower ionosphere, taking into account the realistic STEVE-related SAID condition, is under development by our colleagues and shall be the content of a future publication. From the observational aspect, to check the above theory, an accurate determination of the latitudinal displacement between STEVE and the Picket Fence is required. This would need a high-resolution triangulation analysis using multiple ASIs with overlapping FOV, which we shall attempt as the TREx camera array is fully deployed in the near future.

It is also possible that the motion of the Picket Fence does not follow plasma convection but is related to certain waves/instabilities intrinsic to the ionospheric *E* region. Indeed, the achieved motion velocity of the Picket Fence appears to be close to the typical values of ion acoustic speed in the *E* region. Due to the afore mentioned absence of 427.8 nm emissions in the Picket Fence spectra, it was speculated that the Picket Fence probably represents thermal emissions led by strong turbulence heating in the *E* region (Semeter et al., 2020). Certainly, the SAID electric field sufficiently exceeds the threshold of the Farley-Buneman instability, a widely recognized candidate mechanism of *E* region anomalous heating. However, upon checking the camera data, the apparent width of the Picket Fence structures is estimated to be tens of km (can be inferred from Figures 1 and 2), far larger than the typical meter-scale wavelength of the Farley-Buneman instability, unless the latter is somehow coupled to other longer-wavelength waves (e.g., Young et al., 2017). Also, while it is true that when the nonlinear effect is considered the saturated phase velocity of Farley-Buneman wave can be substantially smaller than the ambient $E \times B$ drift (e.g., Oppenheim et al., 1996), it is still difficult to explain the eastward motion of the Picket Fence if the wave is embedded in an ambient westward flow channel. Therefore, it is fair to state that, so far, there is limited support that Picket Fence structures and their motion could be attributed to an *E* region wave/instability.

The above considerations are admittedly tentative only. To date, the underlying mechanisms of STEVE and the Picket Fence phenomena remain speculative; some of the key chemical/electrodynamic processes are probably not realized so far. Nevertheless, this study reveals that our newly mounted TREx RGB camera can be very useful in studying STEVE and Picket Fence phenomena and our results on the motion of STEVE and the Picket Fence should offer clues to, and impose constraints on, the ongoing exploration of their mechanisms.

## Data Availability Statement

TREx RGB camera data are downloadable online (at http://data.phys.ucalgary.ca/sort_by_project/TREx/RGB/).

**Acknowledgments**

TREx is jointly funded by CFI, Alberta Economic Development and Trade, and the University of Calgary. We thank Dr. J.-P. St.-Maurice, Dr. Martin Connors, and Dr. Brian Harding for helpful discussions.

## References

Anderson, P. C., Carpenter, D. L., Tsuruda, K., Mukai, T., & Rich, F. J. (2001). Multisatellite observations of rapid subauroral ion drifts (SAID). *Journal of Geophysical Research*, *106*(A12), 29,585–29,599. https://doi.org/10.1029/2001JA000128

Archer, W. E., Gallardo-Lacourt, B., Perry, G. W., St. -Maurice, J.-P., Buchert, S. C., & Donovan, E. F. (2019). STEVE: The optical signature of intense subauroral ion drifts. *Geophysical Research Letters*, *46*, 6279–6286. https://doi.org/10.1029/2019GL082687

Archer, W. E., St.- Maurice, J. P., Gallardo-Lacourt, B., Perry, G. W., Cully, C. M., Donovan, E., et al. (2019). The vertical distribution of the optical emissions of a STEVE and Picket Fence event. *Geophysical Research Letters*, *46*, 10,719–10,725. https://doi.org/10.1029/2019GL084473

Baker, K. B., & Wing, S. (1989). A new magnetic coordinate system for conjugate studies at high latitudes. *Journal of Geophysical Research*, *94*(a7), 9139. https://doi.org/10.1029/JA094iA07p09139

Chu, X., Malaspina, D., Gallardo-Lacourt, B., Liang, J., Andersson, L., Ma, Q., et al. (2019). Identifying STEVE's magnetospheric driver using conjugate observations in the magnetosphere and on the ground. *Geophysical Research Letters*, *46*, 12,665–12,674. https://doi.org/10.1029/2019GL082789

Figueiredo, S., Karlsson, T., & Marklund, G. T. (2004). Investigation of subauroral ion drifts and related field-aligned currents and ionospheric Pedersen conductivity distribution. *Annales de Geophysique*, *22*(3), 923–934. https://doi.org/10.5194/angeo-22-923-2004

Gallardo-Lacourt, B., Liang, J., Nishimura, Y., & Donovan, E. (2018). On the origin of STEVE: Particle precipitation or ionospheric skyglow? *Geophysical Research Letters*, *45*, 7968–7973. https://doi.org/10.1029/2018GL078509

Gallardo-Lacourt, B., Nishimura, Y., Donovan, E., Gillies, D. M., Perry, G. W., Archer, W. E., et al. (2018). A statistical analysis of STEVE. *Journal of Geophysical Research: Space Physics*, *123*, 9893–9905. https://doi.org/10.1029/2018JA025368

Gillies, D. M., Donovan, E., Hampton, D., Liang, J., Connors, M., Nishimura, Y., et al. (2019). First observations from the TREx Spectrograph: The optical spectrum of STEVE and the Picket Fence phenomena. *Geophysical Research Letters*, *46*, 7207–7213. https://doi.org/10.1029/2019GL083272

Harding, B. J., Mende, S. B., Triplett, C. C., & Wu, Y.-J. J. (2020). A mechanism for the STEVE continuum emission. *Geophysical Research Letters*, *47*, e2020GL087102. https://doi.org/10.1029/2020GL087102

He, F., Zhang, X.-X., & Chen, B. (2014). Solar cycle, seasonal, and diurnal variations of subauroral ion drifts: Statistical results. *Journal of Geophysical Research: Space Physics*, *119*, 5076–5086. https://doi.org/10.1002/2014JA019807

Hunnekuhl, M., & MacDonald, E. (2019). A citizen science based data package for STEVE phenomenon related subaurora aurora or auroral-like luminous ionospheric structures, (online) 16th European Space Weather Week. Available at: https://register-as.oma.be/esww16/contributions/public/S2-P1/S2-P1-02-HunnekuhlMichael/POSTER1_ESWW.pdf

Hunnekuhl, M., MacDonald, E., Swanson, B., Theusner, M., Stone, J., Chernenkoff, A., et al. (2019). STEVE phenomenon related subauroral aurora or aurora-like luminous ionospheric structures—Relevant structures, characteristics and correlations with geomagnetic storms derived from a citizen science based data package. (online) 16th European Space Weather Week. Available at: https://register-as.oma.be/esww16/contributions/public/S14-P1/S14-P1-05-HunnekuhlMichael/POSTER2_ESWW.pdf

Liang, J., Donovan, E., Connors, M., Gillies, D., St-Maurice, J. P., Jackel, B., et al. (2019). Optical spectra and emission altitudes of double-layer STEVE: A case study. *Geophysical Research Letters*, *46*, 13,630–13,639. https://doi.org/10.1029/2019GL085639

MacDonald, E. A., Donovan, E., Nishimura, Y., Case, N. A., Gillies, D. M., Gallardo-Lacourt, B., et al. (2018). New science in plain sight: Citizen scientists lead to the discovery of optical structure in the upper atmosphere. *Science Advances*, *4*, eaaq0030. https://doi.org/10.1126/sciadv.aaq0030

McCuen, C. H. (1985). *Statistical methods for engineers*. Englewood Cliffs, NJ: Prentice Hall.

Mende, S. B., Harding, B. J., & Turner, C. (2019). Subauroral green STEVE arcs: Evidence for low-energy excitation. *Geophysical Research Letters*, *46*, 14,256–14,262. https://doi.org/10.1029/2019GL086145

Nishimura, Y., Gallardo-Lacourt, B., Zou, Y., Mishin, E., Knudsen, D. J., Donovan, E. F., et al. (2019). Magnetospheric signatures of STEVE: Implication for the magnetospheric energy source and inter-hemispheric conjugacy. *Geophysical Research Letters*, *46*, 5637–5644. https://doi.org/10.1029/2019GL082460

Noël, J., St. -Maurice, J., & Blelly, P. (2000). Nonlinear model of short-scale electrodynamics in the auroral ionosphere. *Annales Geophysicae*, *18*(9), 1128–1144. https://doi.org/10.1007/s00585-000-1128-1

Oppenheim, M., Otani, N., & Ronchi, C. (1996). Saturation of the Farley-Buneman instability via nonlinear electron E×B drifts. *Journal of Geophysical Research*, *101*(A8), 17,273–17,286. https://doi.org/10.1029/96JA01403

Semeter, J., Hunnekuhl, M., Macdonald, E., Hirsch, M., Zeller, N., Chernenkoff, A., & Wang, J. (2020). The mysterious green streaks below STEVE. *AGU Advances*, *2*, e2020AV000183. https://doi.org/10.1029/2020AV000183

Spiro, R., Heelis, R., & Hanson, W. (1979). Rapid subauroral ion drifts observed by Atmospheric Explorer C. *Geophysical Research Letters*, *6*(8), 657–660. https://doi.org/10.1029/GL006i008p00657

St. -Maurice, J.-P., Kofman, W., & James, D. (1996). In situ generation of intense parallel electric fields in the lower ionosphere. *Journal of Geophysical Research*, *101*(A1), 335–356. https://doi.org/10.1029/95JA02586

Sternberg, J. R., & Ingham, M. F. (1972). Observations of the airglow continuum. *Monthly Notices of the Royal Astronomical Society*, *159*(1), 1–20. https://doi.org/10.1093/mnras/159.1.1

Young, M. A., Oppenheim, M. M., & Dimant, Y. S. (2017). Hybrid simulations of coupled Farley-Buneman/gradient drift instabilities in the equatorial *E* region ionosphere. *Journal of Geophysical Research: Space Physics*, *122*, 5768–5781. https://doi.org/10.1002/2017JA024161

Zheng, Y., Brandt, P. C., Lui, A. T. Y., & Fok, M.-C. (2008). On ionospheric trough conductance and subauroral polarization streams: Simulation results. *Journal of Geophysical Research*, *113*, A04209. https://doi.org/10.1029/2007JA012532